2013

Tropical-cyclone flow asymmetries induced by a uniform flow revisited

Montgomery, Michael T.; Davis, Christopher; Dunkerton, Timothy; Wang, Zhuo; Velden, Christopher; Torn, Ryan; Majumdar, Sharanya J.; Zhang, Fuqing; Smith, Roger K.; Bosart, Lance...

Tropical-cyclone flow asymmetries induced by a uniform flow revisited, Monthly Weather Review, in review: 2013, Gerald L. Thomsen, Roger K. Smith, and Michael T. Montgomery

http://hdl.handle.net/10945/36876

Tropical-cyclone flow asymmetries induced by a uniform flow revisited

Gerald L. Thomsen [a], Roger K. Smith [a] *and Michael T. Montgomery [b]
[a] *Meteorological Institute, University of Munich, Munich, Germany,*
[b] *Dept. of Meteorology, Naval Postgraduate School, Monterey, CA & NOAA's Hurricane Research Division*
*Correspondence to: Roger K. Smith, Meteorological Institute, University of Munich, Theresienstr. 37, 80333 Munich, Germany. Email: roger.smith@lmu.de

Idealized, convection-permitting, numerical model simulations are carried out to investigate the hypothesized effects of a uniform flow on the intensification, structural evolution, and maximum intensity of a tropical cyclone. The model used is a modified version of the Pennsylvania State University-National Center for Atmospheric Research fifth-generation Mesoscale Model. For the relatively intense vortices studied here, the differences in intensification rate and mature intensity resulting from changes in the background flow are not significant. As found in previous studies, a uniform flow in conjunction with surface friction leads to an asymmetry in the vertical motion exiting the boundary layer, but in the present experiments, this asymmetry is dominated by transient structures associated with rotating deep convection. Using sets of ensemble experiments in which the initial low-level moisture field is randomly perturbed below a value that can be measured by dropsonde observations, a coherent asymmetry in vertical velocity is evident only for the largest translation speed studied (7.5 m s^{-1}). The maximum vertical motion in the mature stage occurs about 45 degrees to the left of the motion vector, a result that differs from those of previous theoretical studies, which do not explicitly account for deep convection.
The time-mean maximum tangential wind speed occurs on the left side of the storm track as is found in recent observations of boundary-layer flow asymmetries in translating storms. However, the flow variability associated with transient convection raises questions concerning the ability to be able to adequately represent vortex-scale flow asymmetries (especially in the radial direction) from dropwindsonde observations spread over several hours.
The findings are broadly unchanged when using the relatively diffusive Gayno-Seaman boundary-layer parameterization scheme instead of the simpler bulk scheme used for the other calculations.

Key Words: Hurricane; tropical cyclone; typhoon; boundary layer; vortex intensification

Received 27 May 2011; Revised November 9, 2011; Accepted

Citation: . . .

1. Introduction

In a recent paper, Nguyen *et al.* (2008, henceforth M1) investigated the predictability of tropical-cyclone intensification in a three-dimensional numerical model. They focussed on the prototype problem for intensification, which considers the evolution of a prescribed, initially cloud-free, axisymmetric, baroclinic vortex over a warm ocean on an f-plane, and also the corresponding problem on a beta-plane. A complementary study of the same problem

using a minimal three-dimensional model was carried out by Shin and Smith (2008). Both studies found that, on an f-plane, the flow asymmetries that develop are highly sensitive to the initial low-level moisture distribution. When a random moisture perturbation is added in the boundary layer at the initial time, even with a magnitude that is below the accuracy with which moisture is normally measured, the pattern of evolution of the flow asymmetries is dramatically altered and no two such calculations are alike in detail. The same is true also of calculations on a β-plane, at least in the inner-core region of the vortex, within 100-200 km from the centre. Nevertheless the large-scale β-gyre asymmetries remain coherent and are similar in each realization so that they survive when one calculates the ensemble mean. The implication is that the inner-core asymmetries on the f- and β-plane result from the onset of deep convection in the model and that, like deep convection in the atmosphere, they have a degree of randomness, being highly sensitive to small-scale inhomogeneities in the low-level moisture distribution. Such homogeneities are a well-known characteristic of the real atmosphere (e.g. Weckwerth, 2000).

In the foregoing flow configurations, there was no ambient flow and an important question remains: could the imposition of a uniform flow or a vertical shear flow lead to an organization of the inner-core convection, thereby making its distribution more predictable? For example, there is evidence from observations (Kepert 2006a,b, Schwendike and Kepert 2008) and from a simple and more sophisticated boundary layer models (Shapiro, 1983, Kepert 2001, Kepert and Wang 2001) that a translating vortex produces a distinct asymmetric pattern of low-level convergence and vertical motion. There is much evidence also that vertical shear induces an asymmetry in vortex structure (Raymond 1992, Jones 1995, 2000a,b, Smith *et al.* 2000, Frank and Ritchie 1999, 2001, Reasor and Montgomery 2001, 2004, Corbosiero and Molinari 2002, 2003, Riemer *et al.* 2010). An important observational study by Corbosiero and Molinari (2003) showed that the distribution of strong convection is more strongly correlated with the vertical shear than with the storm translation vector. Nevertheless, the question remains as to what happens in the weak shear case and whether the storm translation can be a pertinent process in organizing convection in these circumstances.

As noted in M1 and in Shin and Smith (2008), the random nature of the inner-core asymmetries calls for a new methodology to assess differences between two particular flow configurations, because the results of a single deterministic calculation in each configuration may be unrepresentative of a model ensemble in each configuration. That means one needs to compare the ensemble means of suitably perturbed ensembles of the two configurations. We apply this methodology here to extend the calculations of M1 to the prototype problem for a moving vortex. This problem considers the evolution of an initially dry, axisymmetric vortex embedded in a uniform zonal flow on an f-plane.

Even in the relatively simple case of a uniform flow, there is some disagreement in the literature on the orientation of flow asymmetries that materialize. For example, using a nonlinear, slab boundary layer model with constant depth, Shapiro (1983) shows that the strongest convergence (and hence vertical velocity in his model) occurs on the forward side of the vortex in the direction of motion (see his Figures 5d and 6c). In contrast, the purely linear theory of Kepert (2001, left panel of Figure 5) predicts that the strongest convergence lies at 45 degrees to the right of the motion and the nonlinear calculations of Kepert and Wang (2001, bottom left panel of Figure 10) predicts it to be at 90 degrees to the right of motion. As noted by the respective authors, a limitation of the foregoing studies is the fact that the horizontal flow above the boundary layer is prescribed and not determined as part of a full solution.

Here we seek to answer the questions:

1 Does the imposition of a uniform flow in a convection-permitting simulation lead to an organization of the inner-core convection so as to produce persistent asymmetries in convergence and vertical motion?
2 Does the imposition of a uniform flow significantly affect the intensification rate and mature intensity for storm translation speeds typical of those in the tropics?
3 If so, are these asymmetries similar to those predicted by earlier studies where the horizontal flow above the boundary layer is prescribed?
4 How do the asymmetries in low-level flow structure associated with the storm translation compare with those documented in recent observational studies?

We are aware of three previous modelling studies addressing the second question above (Dengler and Keyser 1999, Peng *et al.* 1999, Wu and Braun 2004). All three studies found a systematic reduction of intensity with translation speed. Peng *et al.* attributed this reduction to an out of phase relationship between the asymmetry in surface moisture flux and boundary-layer moisture convergence. In contrast, Dengler and Keyser found that, in their three-layer model, it was the penetration of stable dry air from mid-levels to the boundary layer that reduced the storm intensity. Finally, Wu and Braun (2004) suggested that the inhibiting effect of an environmental flow is closely associated with the resulting eddy momentum flux, which tends to decelerate tangential and radial winds in both inflow and outflow layers. The corresponding changes in the symmetric circulation tend to counteract the deceleration effect. The net effect is a moderate weakening of the mean tangential and radial winds. Interestingly, the first two of these studies give thermodynamic arguments for the vortex behaviour in a mean flow while the third gives an interpretation based on dynamical processes.

All of these studies used models employing a relatively coarse horizontal resolution by today's standards (Peng *et al.* used 0.5^o latitude, Dengler and Keyser used 20 km, Wu and Braun used 25 km) and relied on a parameterization of deep cumulus convection. Both Peng *et al.* and Wu and Braun used the Kuo scheme, which has been heavily criticized* because of its use of moisture convergence as the basis for its closure. Dengler and Keyser used the simple scheme proposed by Ooyama (1969) in which the cloud-base mass flux is equal to the resolved-scale mass flux in the boundary layer. Because of the uncertainties underlying the parameterization of deep convection in these studies, and because of recent insights into the role of deep convection on tropical-cyclone intensification that have emerged in the last few years, it seems appropriate to revisit

*See Raymond and Emanuel (1993).

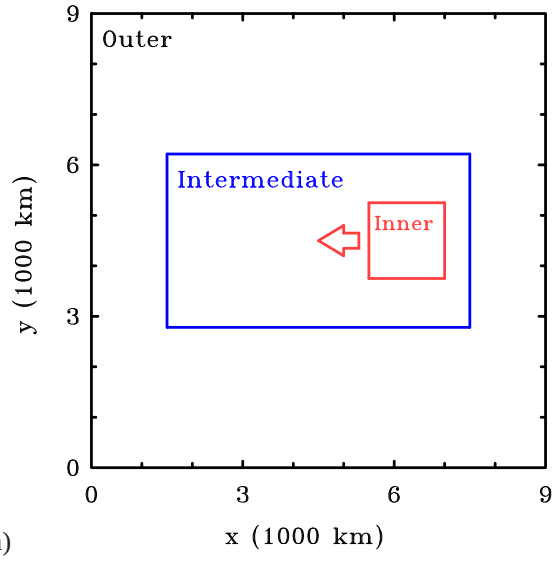

(a)

Figure 1. Configuration of the three model domains. The inner domain is moved from east to west (the negative x-direction) at selected times to keep the vortex core away from the domain boundary.

question [2] above. In fact, Wu and Braun recommend further investigation of the various physical mechanisms responsible for tropical-cyclone intensity (resulting from large-scale influences) using high-resolution simulations with more sophisticated model physics.

The remainder of the paper is structured as follows. In section 2 we give a brief description of the model and in section 3 we present the results of the main calculations for vortex evolution on an f-plane and in section 4 we describe the ensemble experiments, where, as in M1, the ensembles are generated by adding small moisture perturbations at low levels. Section 5 examines the asymmetric structure of boundary layer winds and section 6 describes briefly a calculation using a different boundary-layer scheme. The conclusions are given in section 7.

2. The model configuration

The numerical experiments are similar to those described in M1 and are carried out also using a modified version of the Pennsylvania State University-National Center for Atmospheric Research fifth-generation Mesoscale Model (MM5; version 3.6, Dudhia 1993; Grell *et al.* 1995). The model is configured with three domains with sides orientated east-west and north-south (Figure 1). The outer and innermost domains are square, the former 9000 km in size and the latter 1500 km. The innermost domain is moved from east to west at selected times within an intermediate domain with zonal dimension 6000 km and meridional dimension 3435 km. The first displacement takes place 735 minutes after the initial time and at multiples of 1440 minutes (one day) thereafter. The distance displaced depends on the background wind speed in the individual experiments. The outer domain has a relatively coarse, 45-km, horizontal grid spacing, reducing to 15 km in the intermediate domain and 5 km in the innermost domain. The two inner domains are two-way nested. In all calculations there are 24 σ-levels in the vertical, 7 of which are below 850 mb. The model top is at a pressure level of 50 mb. The calculations are performed on an f-plane centred at 20 °N.

In order to keep the experiments as simple as possible, we choose the simplest explicit moisture scheme, one that mimics pseudo-adiabatic ascent[†]. In addition, for all but one experiment we choose the bulk-aerodynamic parameterization scheme for the boundary layer. An additional calculation is carried out using the Gayno-Seaman boundary-layer scheme (Shafran *et al.* 2000) to investigate the sensitivity of the results to the particular scheme used.

The surface drag and heat and moisture exchange coefficients are modified to incorporate the results of the coupled boundary layer air-sea transfer experiment (CBLAST; see Black *et al.* 2007, and Zhang *et al.* 2009). The surface exchange coefficients for sensible heat and moisture are set to the same constant, 1.2×10^{-3}, and that for momentum, the drag coefficient, is set to $0.7 \times 10^{-3} + 1.4 \times 10^{-3}(1 - \exp(-0.055|\mathbf{u}|))$, where $|\mathbf{u}|$ is the wind speed at the lowest model level. The fluxes between the individual model layers within the boundary layer are then calculated by a first-order (local K-mixing) scheme.

The exchange coefficient for moisture is set to zero in the two outer domains to suppress the build up there of environmental Convective Available Potential Energy (CAPE). Because of the dependence of the moisture flux on wind speed, such a build up would be different in the experiments with different wind speeds. In all except one experiment, the sea surface temperature is set to a constant 27^{o}C. In the remaining experiment it was set to 25^{o}C to give a weaker mature vortex. The radiative cooling is implemented by a Newtonian cooling term that relaxes the temperature towards that of the initial profile on a time scale of 1 day. This initial profile is defined in pressure coordinates rather than the model's σ-coordinates in order to not induce a thermal circulation between southern and northern side of the model domain.

In each experiment, the initial vortex is axisymmetric with a maximum tangential wind speed of 15 m s^{-1} at the surface at a radius of 120 km. The strength of the tangential wind decreases sinusoidally with height, vanishing at the top model level (50 mb). The vortex is initialized to be in thermal wind balance with the wind field using the method described by Smith (2006). The far-field temperature and humidity are based on Jordan's Caribbean sounding (Jordan 1958). The vortex centre is defined as the centroid of relative vorticity at 900 mb over a circular region of 200 km radius from a "first-guess" centre, which is determined by the minimum of the total wind speed at 900 mb.

2.1. *The main experiments*

Four main experiments are discussed, three with a uniform background easterly wind field, U, and the other with zero background wind. All these experiments employ the bulk aerodynamic representation of the boundary layer and have

[†]If the specific humidity, q, of a grid box is predicted to exceed the saturation specific humidity, $q_s(p, T)$ at the predicted temperature T and pressure p, an amount of latent heat $L(q - q_s)$ is converted to sensible heat raising the temperature by $dT = L(q - q_s)/c_p$ and q is set equal to q_s, so that an amount of condensate $dq = q - q_s$ is produced. (Here L is the coefficient of latent heat per unit mass and c_p is the specific heat of air at constant pressure.) The increase in air parcel temperature increases q_s, so that a little less latent heat than the first estimate needs to be released and a little less water has to be condensed. The precise amount of condensation can be obtained by a simple iterative procedure. Convergence is so rapid that typically no more than four iterations are required.

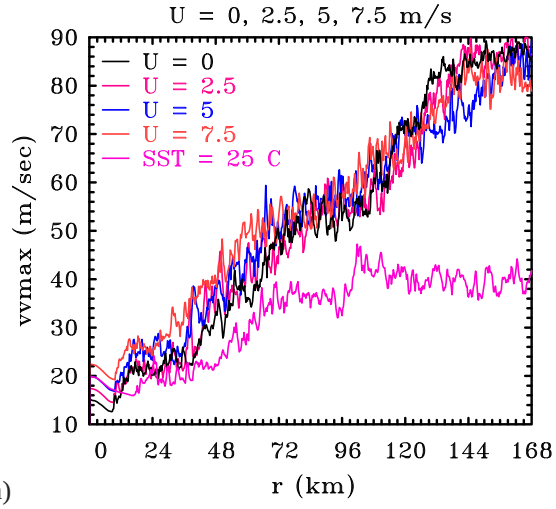

(a)

Figure 2. Time series of maximum total wind speed at 850 mb for (a) four experiments with variable background wind speed (black: $U = 0$ m s^{-1}, red: $U = 2.5$ m s^{-1}, blue: $U = 5.0$ m s^{-1}, purple: $U = 7.5$ m s^{-1} and for an experiment with $U = 5.0$ m s^{-1} but with the sea surface temperature reduced to 25^{o}C.

a sea surface temperature of 27^{o}C. Values of U are 2.5 m s^{-1}, 5 m s^{-1}, and 7.5 m s^{-1}, adequately spanning the most common range of observed tropical-cyclone translation speeds. Two additional experiments have $U = 5$ m s^{-1}, one with a sea surface temperature of 25^{o}C to give a weaker vortex and the other with the Gayno-Seaman boundary-layer scheme.

2.2. *Ensemble experiments*

As in M1, sets of ensemble calculations are carried out for the main experiments. These are similar to the main calculations, but have a ± 0.5 g kg^{-1} random perturbation added to the water-vapour mixing ratio up to 950 mb at the initial time. In order to keep the mass field unchanged, the temperature is adjusted at each point to keep the virtual temperature unchanged. A four member ensemble was carried out for $U = 0$ m s^{-1} and $U = 7.5$ m s^{-1} and a ten member ensemble for $U = 5$ m s^{-1}.

3. Results of five deterministic calculations

3.1. *Vortex evolution*

Figure 2 shows time-series of the maximum total wind speed, VT_{max} at 850 mb (approximately 1.5 km high) during a 7 day (168 hour) integration in the four main experiments and in that with a background flow of 5 m s^{-1} and a sea surface temperature of 25^{o}C. The last experiment will be discussed in section 3.3. As in many previous experiments, including those in M1, the evolution begins with a gestation period during which the vortex slowly decays due to surface friction, but moistens in the boundary layer due to evaporation from the underlying sea surface. This period lasts approximately 9 hours during which time the maximum total wind speed decreases by about 2.0 m s^{-1}.

The imposition of friction from the initial instant leads to inflow in the boundary layer and outflow above it, the outflow accounting for the decrease in tangential wind speed through the conservation of absolute angular momentum. The inflow is moist and as it rises out of the boundary layer and cools, condensation progressively occurs in some grid columns interior to the corresponding radius of maximum tangential wind speed. Existing relative vorticity is stretched and amplified in these columns leading to the formation of localized rotating updraughts. Hendricks *et al.* (2004) coined the term "vortical hot towers" for these updraughts.

As the updraughts develop, there ensues a period lasting about 5 days during which the vortex progressively intensifies. During this time, VT_{max} increases from its minimum value of between 12.5 and 20 m s^{-1} to a final value of between 80 and 90 m s^{-1} at the end of the experiment. The vortex in the quiescent environment is the first to attain a quasi-steady state after about 6 days, but all appear to have reached such a state after 7 days. Note that for all values of U, there are large fluctuations in VT_{max}, up to ± 5 m s^{-1}, during the period of intensification. Indeed, for most of the time, the fluctuations of an individual experiment are comparable with the maximum deviations between the different experiments, so much so that it is reasonable to ask if the differences between the four experiments are significant. We examine this important question in section 4.1.

3.2. *Structure changes*

The evolution in vortex structure during the intensification stage is exemplified by the contours of vertical velocity at 850 mb at selected times for the main experiment with $U = 5$ m s^{-1}. These contours are shown in Figures 3 and 4. At early times, convective cells begin to develop in the forward left (i.e. southwest) quadrant, where, as shown below, the boundary-layer-induced convergence is large (Figure 3a). However, cells subsequently develop clockwise (upstream) in the space of two hours to the forward quadrant (Figure 3b) and over the next two hours to the forward right and rear right quadrants (Figure 3d). It should be emphasized that, as in the calculations in M1, the cells are rotating faster than their local environment and they are deep, extending into the upper troposphere (not shown here).

By 24 hours, convective cells are distributed over all four quadrants with little obvious preference for a particular sector. Moreover, they amplify the vertical component of local low-level relative vorticity by one or two orders of magnitude. For comparison, panels (e) and (f) of Figure 3 show the early evolution of cells in the main calculation with zero background flow, which, as expected, shows no preference for cells to develop in a particular sector.

As time proceeds, the convection becomes more organized (Figure 4), showing distinctive banded structures, but even at 90 hours, its distribution is far from axisymmetric, even in the region within 100 km of the axis. However, as shown later, the vortex does develop an annular ring of convection with an eye-like feature towards the end of the integration.

Figure 5 shows the pattern of convergence at a height of 500 m averaged between 3 and 5 h and 6.5-7 days in the case with $U = 5$ m s^{-1}. This height is typically that of the maximum tangential wind speed and about half that of the 'mean' inflow layer in the mature stage (see section 5). The period 3-5 hours is characteristic of the gestation period during which the boundary layer is moistening, but before convection has commenced. During

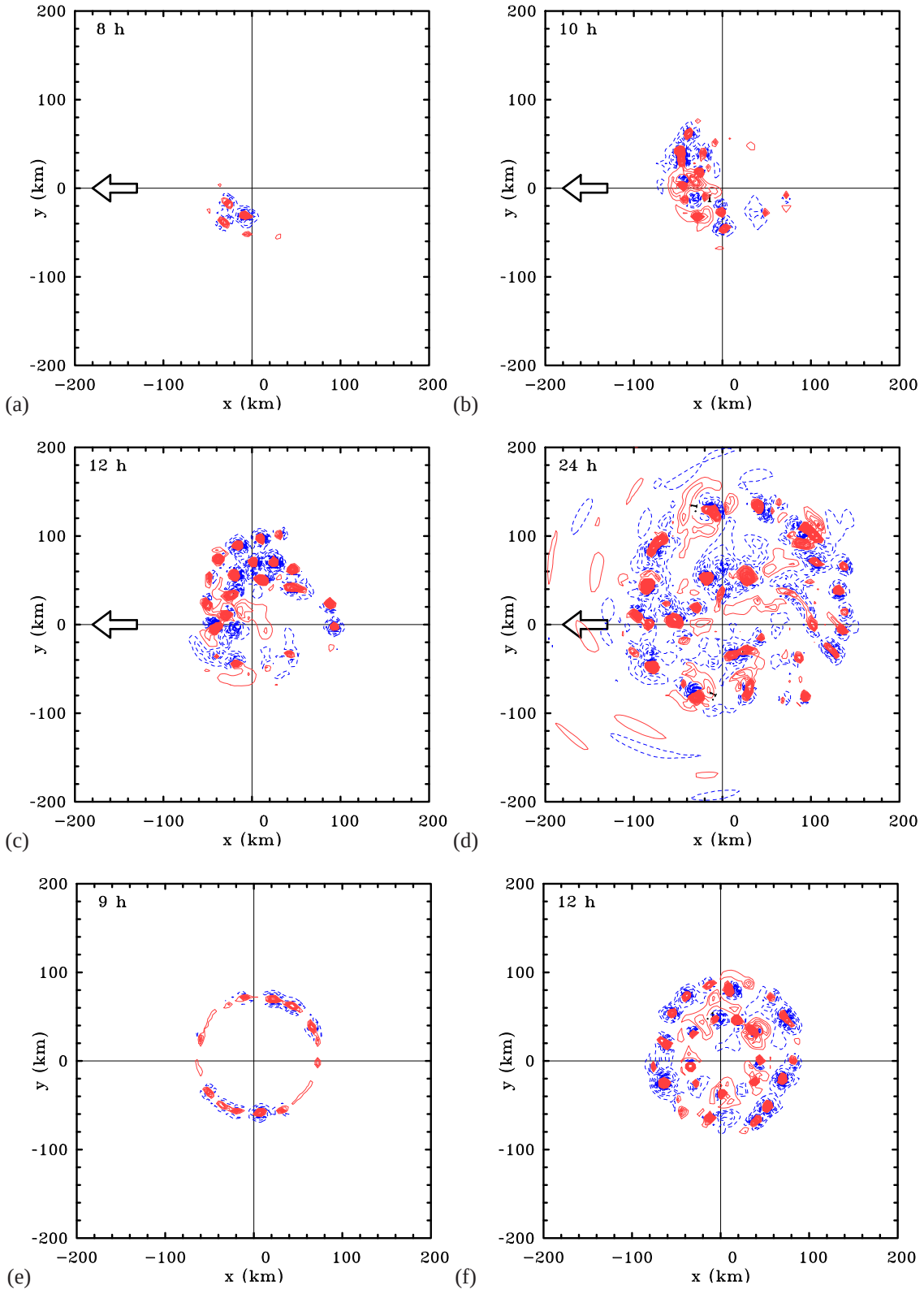

Figure 3. Contours of vertical velocity at 850 mb at times indicated in the top right of each panel during the vortex evolution. (a)-(d) for the experiment with $U = 5.0$ m s^{-1} (from right to left), and (e) and (f) for the experiment with the zero background flow. Contour interval: thick contours 0.5 m s^{-1}, thin contours 0.1 m s^{-1}. Positive velocities (solid/red lines), negative velocities (dashed/blue lines). The arrow indicates the direction of vortex motion.

this period, the convergence is largest on the forward side of the vortex, explaining why the convective instability is first released on this side. There is a region of divergence in the rear left sector. The pattern is similar to that predicted by Shapiro (1983: see his Figure 5d and note that it is oriented differently to ours in respect to the translation direction), but in Shapiro's calculation, which, at this stage was for a stronger symmetric vortex with a maximum tangential wind speed of 40 m s^{-1} translating at a speed of 10 m s^{-1}, the divergence region extends also to the rear right of the track.

In the mature stage in our calculation the pattern of convergence is rather different to that in Shapiro's

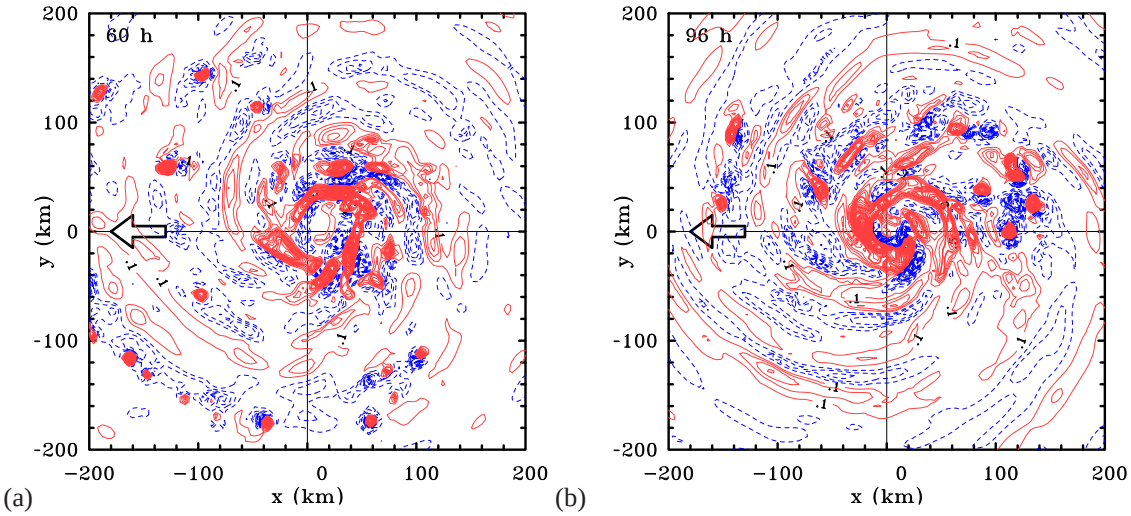

Figure 4. Contours of vertical velocity at 850 mb at (a) 60 hours, and (b) 96 hours, during the vortex evolution for the experiment with $U = 5.0$ m s^{-1} (from right to left). Contour interval: thick contours 0.5 m s^{-1}, thin contours 0.1 m s^{-1}. Positive velocities (solid/red lines), negative velocities (dashed/blue lines). The arrow indicates the direction of vortex motion.

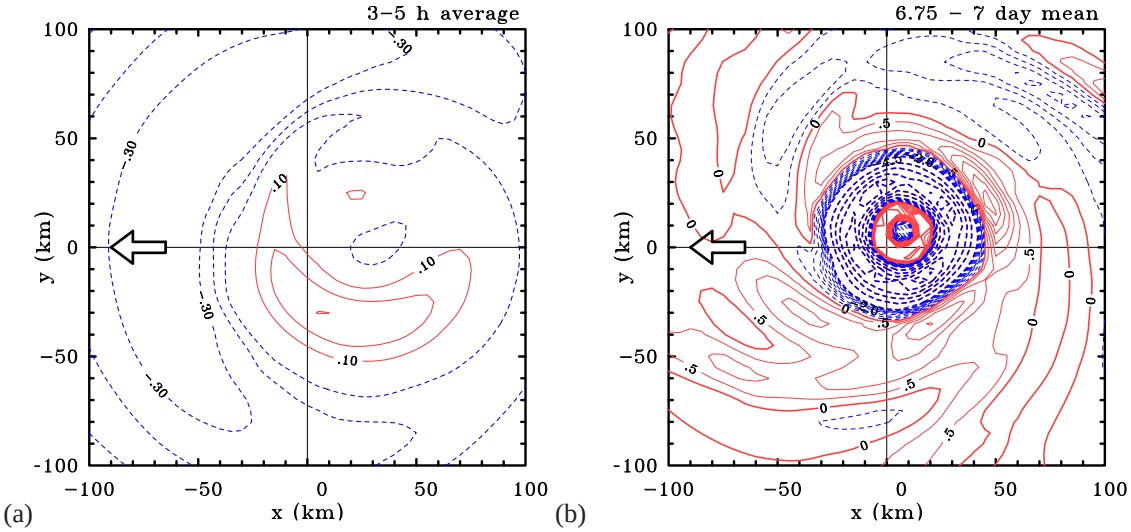

Figure 5. Contours of divergence at 500 m at for the experiment with $U = 5.0$ m s^{-1}: (a) between 3-5 hours (contour interval 1×10^{-5} s^{-1}. Positive contours (solid/red) and negative values (dashed/blue).) and (b) between $6\frac{3}{4} - 7$ days (contour interval: thick contours 5×10^{-4} s^{-1}, thin contours 5×10^{-5} s^{-1}. Positive contours (solid/red) and negative values (dashed/blue)). The arrow indicates the direction of vortex motion.

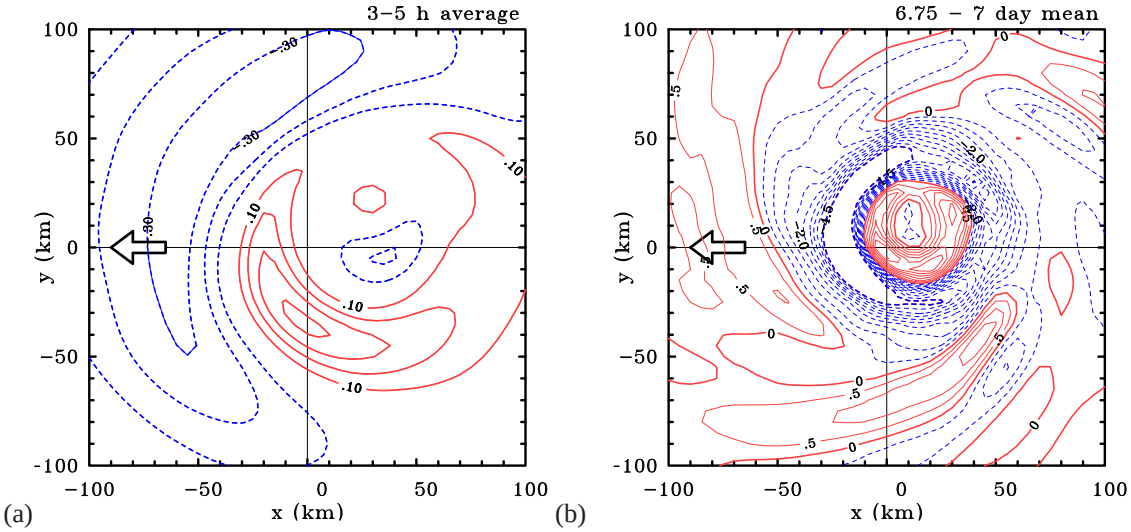

Figure 6. Contours of divergence at 500 m at for the experiment with $U = 5.0$ m s^{-1} and a sea surface temperature of 25^{o}C: (a) between 3-5 hours (contour interval 1×10^{-5} s^{-1}). (b) between $6\frac{3}{4} - 7$ days (contour interval: thick contours 5×10^{-4} s^{-1}, thin contours 5×10^{-5} s^{-1}. Positive contours (solid/red) and negative values (dashed/blue). The arrow indicates the direction of vortex motion.

calculation and is much more symmetric, presumably because at this stage the vortex is twice as strong as Shapiro's and the translation speed is only half. Notably, outside the ring of strong convergence that marks the eyewall, the vortex is almost surrounded by a region of low-level divergence, except for the narrow band of convergence feeding into the eyewall on the forward right side. In the next section we examine the differences in behaviour for a weaker vortex.

3.3. *Calculations for a weaker vortex*

To examine the questions raised in the previous section concerning possible differences when the vortex is much weaker, we repeated the experiment with $U = 5$ m s^{-1} with the sea surface temperature reduced by 2^{o}C to 25^{o}C. Figure 2 shows the variation of total wind speed at 850 mb in this case. As expected, the evolution is similar to that in Figure 3, but the maximum wind speed during the mature stage is considerably reduced, with the average wind speed during the last 6 hours of the calculation being only about 40 m s^{-1}. Figure 6 shows the patterns of divergence at a height of 500 m averaged during 3-5 hours and during the last 6 hours of the calculation. These should be compared with the corresponding fields in Figure 5. In the early period (panel (a)), the patterns are much the same, although the maximum magnitudes of divergence and convergence are slightly larger when the sea surface temperature is reduced. We have no explanation for this difference, but do not consider it to be significant. In the mature stage (panel (b)), the differences are considerable with the central ring of divergence marking the eye being much larger in the case of the weaker vortex and the region of convergence surrounding it and marking the eyewall being broader and more asymmetric. However, like the stronger vortex and that in Shapiro's calculation, the largest convergence is on the forward side of the vortex with respect to its motion.

4. Ensemble experiments

As pointed out by M1 and Shin and Smith (2008), the convective nature of the vortex evolution and the stochastic nature of deep convection, itself, means that the vortex asymmetries will have a stochastic component also. Thus, a particular asymmetric feature brought about by an asymmetry in the broadscale flow (in our case the uniform flow coupled with surface friction) may be regarded as significant only if it survives in an ensemble of experiments in which the details of the convection are different. For this reason, we carried out a series of ensemble experiments in which a random moisture perturbation is added to the initial condition in the main experiments as described in section 2.2. We begin by investigating the effects of this stochastic component on the vortex intensification and go on to examine the effects on the vortex structure in the presence of uniform flows with different magnitudes.

4.1. *Stochastic nature of vortex evolution*

Figure 7a shows time series of maximum total wind speed at 850 mb for the main experiment with a background flow of 5 m s^{-1} and ten ensembles thereof. There are several features of interest:

- Intensification in the ensemble experiments begins about an hour earlier than in the main experiment;
- There is a significant difference between the maximum and minimum intensity at any one time, being as high as 12 m s^{-1} during the intensification phase.
- There are times when the intensity in the main experiment is appreciably larger than the ensemble mean at some times and appreciably less at others.
- The mature intensity in the main experiment is about 5 m s^{-1} more than the ensemble mean intensity.

It is clear that differences in intensity between the main experiments with different values of background flow shown in Figure 2 may not be significant. This possibility is explored with the help of Figure 7b, which shows similar time series for the main calculations with $U = 0$ m s^{-1}, $U = 5$ m s^{-1}, and $U = 7.5$ m s^{-1} and four ensembles thereof (comparison of the curves for $U = 5$ m s^{-1} with those in panel (a) suggests that four ensembles together with the corresponding control experiment give a reasonable span of the range of variability in this case). The fact that there is considerable overlap between the envelope of ensembles for different values of U suggests that the differences in intensity for the different values of U are not significant. Indeed, they would lie well within the uncertainty of current operational intensity forecasts.

When viewed in the proper way, the foregoing results are consistent with those of Zeng *et al.* (2007), who presented observational analyses of the environmental influences on storm intensity and intensification rate based on reanalysis and best track data of Northwest Pacific storms. While they considered a broader range of latitudes, up to 50^{o}N, and of storm translation speeds of up to 30 m s^{-1}, the data that are most relevant to this study pertain to translation speeds between 3 and 8 m s^{-1}. The most intense tropical cyclones and those with the most rapid intensification rates were found to occur in this range when there is relatively weak vertical shear. Most significantly, their data have a lot of scatter in this range and do not show an obvious relationship between intensity and translation speed.

4.2. *Stochastic nature of vortex structure*

Figure 8 shows the time-averaged vertical velocity fields for the last 6 hours of integration ($6\frac{3}{4}$ - 7 days) in three of the experiments with $U = 5.0$ m s^{-1}, including the main experiment and two ensemble experiments. It shows also the eleven-member ensemble mean. Perhaps the most prominent asymmetry in the maximum vertical motion is at azimuthal wavenumber-4, which is a feature also of the ensemble mean of calculations for a quiescent environment (panel (e)). As the latter would be expected to have no asymmetry for a sufficiently large ensemble, we are inclined to conclude that the wavenumber-4 asymmetry in this case is at least partially a feature of the low ensemble sample and possibly also of the limited grid resolution (the 100 km square domain in Figure 8 is spanned by only 21×21 grid points). Therefore we do not attribute much significance to the wavenumber-4 component of the asymmetry in panels (a)-(d). Indeed, this asymmetry is less pronounced in the mean of the eleven calculations shown in panel (d). The preference for enhanced ascent in the forward left quadrant is largest in the mean of five calculations for $U = 7.5$ m s^{-1} shown in panel (f).

On the basis of these results, we are now in a position to answer the first of the three questions posed in the

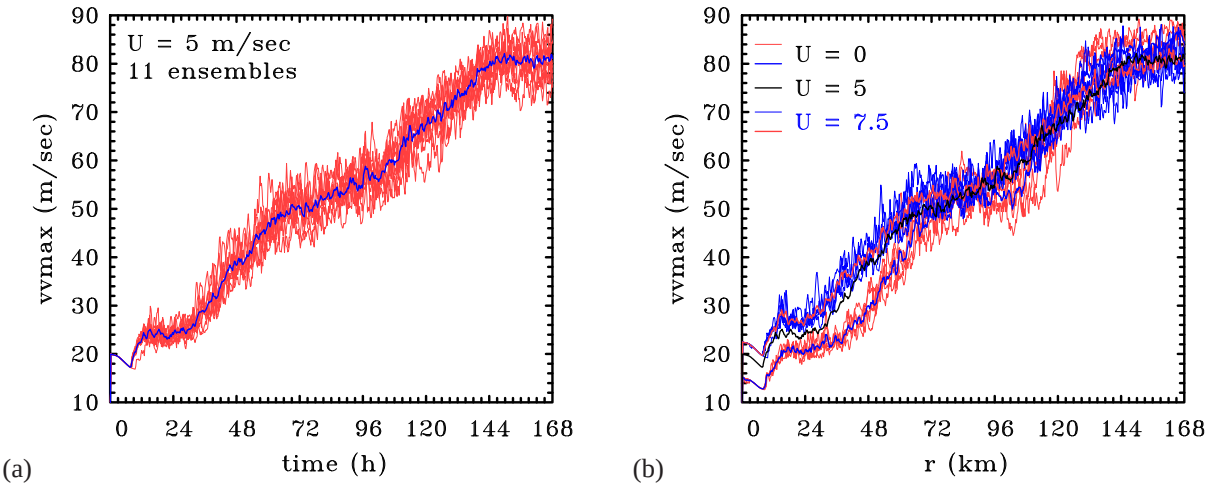

Figure 7. (a) Time series of maximum total wind speed at 850 mb for the main experiment with a background flow of 5 m s^{-1} (thick black curve) and the ten ensemble experiments (thin red curves). The thick blue curve is the mean of the eleven maxima at a given time. (b) Similar time series for the three of the main experiments: the one with zero background wind speed and the other two with background wind speeds $U = 5.0$ m s^{-1} and $U = 7.5$ m s^{-1}. The thin curves show the time series for four ensembles of each of these experiments. The thick curves show the mean of each experiment and the four ensembles.

Introduction: does the imposition of a uniform flow in a convection-permitting simulation lead to an organization of the inner-core convection so as to produce asymmetries in low-level convergence and vertical motion? The answer to this question is a qualified yes, the qualification being that the effect is at most tiny, at least for the strong vortices that arise in our calculations and translation speeds below about 5 m s^{-1}, although it does increase with translation speed. Indeed a more prominent azimuthal wavenumber-1 asymmetry was found in the calculation for a weaker storm (see section 3.3 and Figure 6b).

We are in a position also to answer the third of three questions: how do the asymmetries compare with those predicted by earlier studies? For the modest translation speed (5 m s^{-1}), the ensemble mean vertical velocity asymmetry, which is in the forward left quadrant in our calculations, is closest to the prediction of Shapiro (1983). Whereas, Shapiro found the maximum convergence (and hence vertical motion in his slab model) to be directly ahead of the motion vector, we find it to be approximately 45^o to the left thereof. Our result deviates significantly from that in Kepert's (2001) linear theory, where the maximum vertical motion is at 45^o to the right of the motion vector and even more from that in the nonlinear numerical calculation of Kepert and Wang (2001), where the maximum is at 90^o to the right of the motion vector. The reasons for these discrepancies are unclear, but they could be because, in our calculations, the vortex flow above the boundary layer is determined as part of a full solution for the flow and is not prescribed. Nevertheless, this reason would not account for the discrepancies between Shapiro's results and those of Kepert (2001) and Kepert and Wang (2001). Although the last two papers cited Shapiro's earlier work, they did not comment on the differences between their findings and his.

4.3. *Wind asymmetries*

Figure 9 shows contours of Earth-relative *total wind speed* at 850 mb averaged during the period $6\frac{3}{4} - 7$ days about the centre of minimum total wind speed at this level for the control experiment with $U = 5.0$ m s^{-1}, two ensembles for this value and the ensemble mean (control + ten ensembles). As might be expected, the largest wind speed occurs on the right of the track, but in the forward right sector rather than exactly on the right as would be the case for the tangential velocity component for a translating barotropic vortex in a uniform flow. Note that the maximum is less in ensemble 2 (panel (c)) than in ensemble 1 (panel (b)) and larger in ensemble 1 than in the control experiment (panel (a)). Significantly, the maximum in the forward right quadrant survives in the ensemble mean, again an indication that this maximum is a robust asymmetric feature.

Figure 10 shows the contours of total wind speed at 850 mb in a co-moving (*i. e.*, storm-relative) frame, again averaged during the period $6\frac{3}{4} - 7$ days, in the control experiment (panel (a)) and in the ensemble mean (panel (b)). In this frame, the maximum wind speed for the experiments with $U = 5.0$ m s^{-1} lies around the two left sectors in the direction of motion. The lower panels of Figure 10 show the corresponding pattern of isotachs when the background flow is increased to 7.5 m s^{-1}. In this case the location of maximum total wind moves to the forward sector. This feature is consistent with Shapiro's Figures 5c and 6b, but perhaps less pronounced because of the larger intensity and fractionally smaller translation speed in our case.

5. Asymmetry of boundary-layer winds

We seek now to answer the third question posed in the Introduction. In a series of papers, Kepert (2006a,b) and Schwendike and Kepert (2008) carried out a detailed analysis of the boundary-layer structure of four hurricanes based on Global Positioning System dropwindsonde measurements, complementing the earlier observational study of Powell (1982). Amongst the effects noted by Kepert (2006a) for Hurricane Georges (1998) were that the low-level maximum of the tangential wind component "becomes closer to the storm centre and is significantly stronger (relative to the flow above the boundary layer) on the left of the storm than the right". He noted also that "there is a tendency for the boundary-layer inflow to become deeper and stronger towards the front of the storm, together with the formation of an outflow layer above,

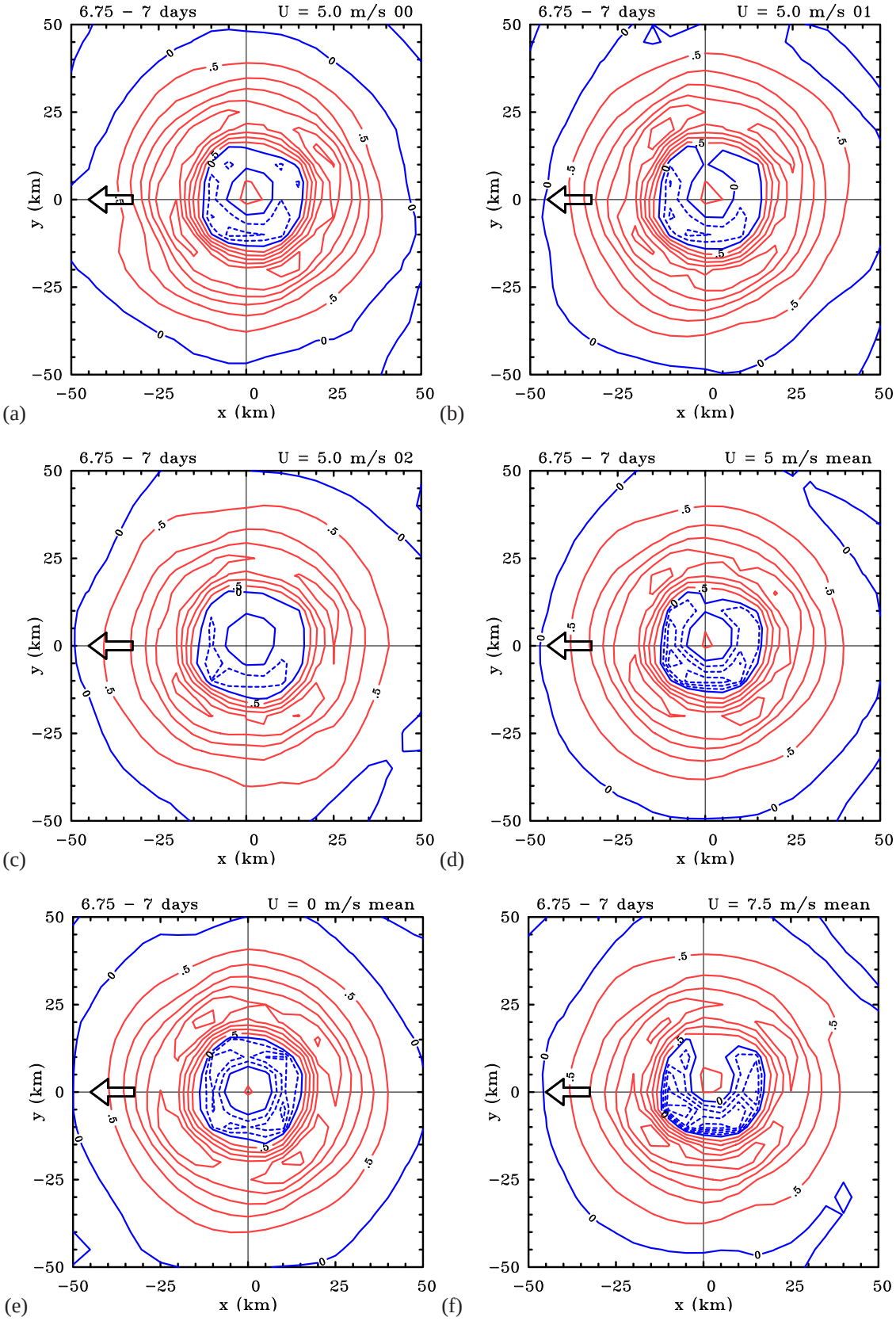

Figure 8. Contours of vertical velocity at 850 mb averaged during the period $6\frac{3}{4} - 7$ days about the centre of minimum total wind speed at this level in the experiments with $U = 5.0$ m s^{-1}. (a) The main experiment; (b) and (c) two ensemble experiments, and (d) the average of the main and ten ensemble experiments. For comparison, panels (e) and (f) show the mean fields (main experiment plus four ensembles) for the experiment with no background flow and that for $U = 7.5$ m s^{-1}, respectively. Contour interval 0.5 m s^{-1}. Positive velocities (solid/red lines), negative velocities (dashed/blue lines). The arrow indicates the direction of vortex motion.

which persists around the left and rear of the storm." We examine now whether such features are apparent in the present calculations.

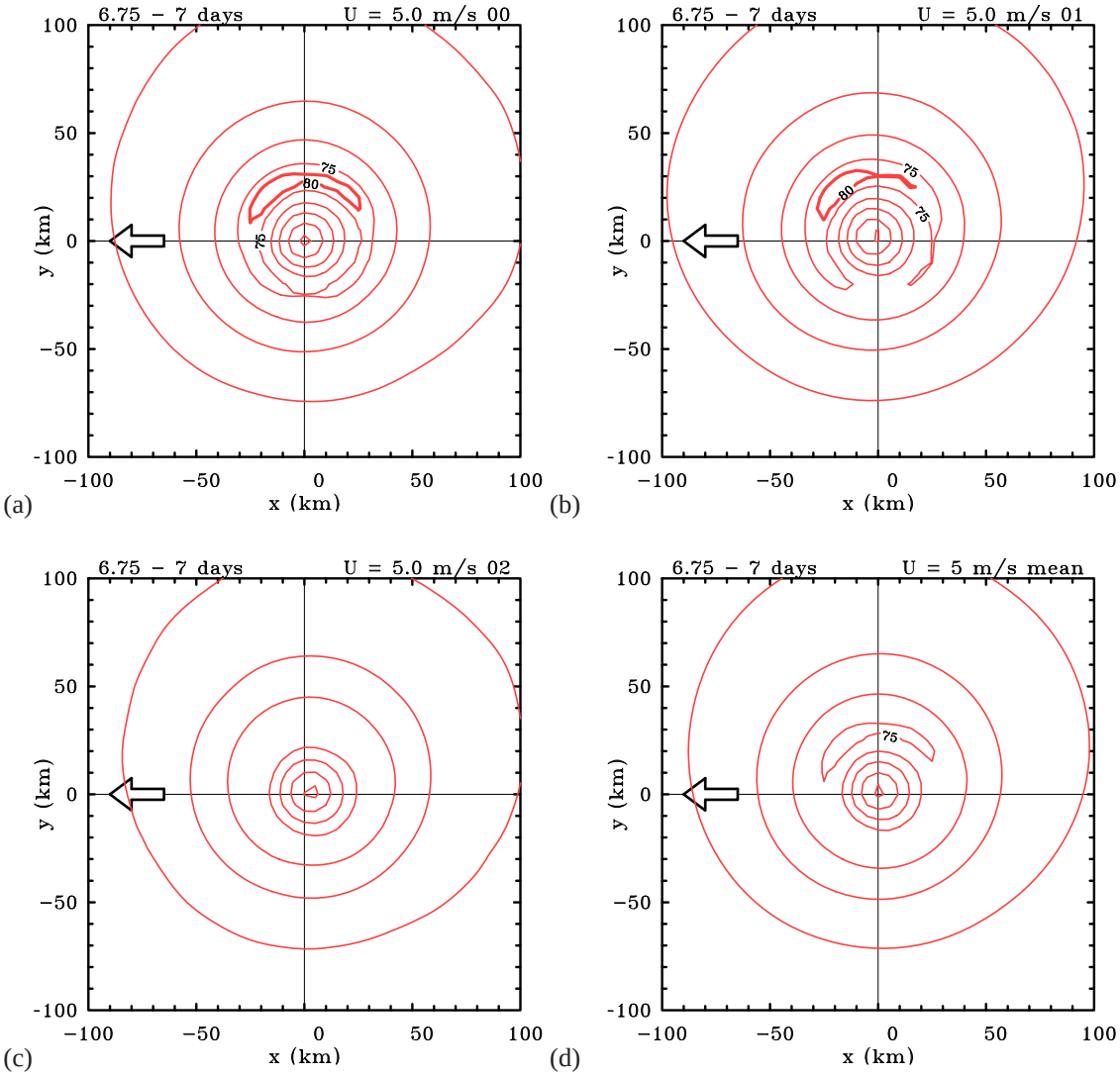

Figure 9. Contours of Earth-relative total wind speed at 850 mb averaged during the period $6\frac{3}{4} - 7$ days about the centre of minimum total wind speed at this level. (a) the main experiment and (b), (c) two ensemble experiments with $U = 5.0$ m s^{-1}. Panel (d) shows the average of the main and ten ensemble experiments. Contour interval 15 m s^{-1} (thin contours). The thick contour in panels (a) and (b) has the value 80 m s^{-1}. The arrow indicates the direction of vortex motion.

Figure 11 shows height-radius cross sections of the tangential and radial wind component in the co-moving frame in different compass directions for the main calculation with $U = 5$ m s^{-1}. Panels (a) and (b) of this figure show time-averaged isotachs of the tangential winds in the last six hours of the calculation in the west-east (W-E) and south-north (S-N) cross sections to a height of 3 km. These do show a slight tendency for the maximum tangential wind component at a given radius to become lower with decreasing radius as the radius of the maximum tangential wind is approached. Moreover, the maximum tangential wind speed occurs on the left (i.e. southern) side of the storm as found by Kepert. The maximum wind speeds in the various compass directions are: W 77.1 m s^{-1}, SW 85.9 m s^{-1}, S 85.9 m s^{-1}, SE 84.0 m s^{-1}, E 78.3 m s^{-1}, NE 73.7 m s^{-1}, N 71.0 m s^{-1}, NW 73.9 m s^{-1}. Thus the highest wind speeds extend across the sector from southwest to southeast and the lowest winds in the sector northeast to northwest.

Panels (c)-(f) of Figure 11 show the corresponding time-averaged isotachs of the radial winds in the west-east, southwest-northeast (SW-NE), south-north and southeast-northwest (SE-NW) cross sections. The maximum radial wind speeds in the various compass directions are: W 43.5 m s^{-1}, SW 39.3 m s^{-1}, S 34.8 m s^{-1}, SE 29.7 m s^{-1}, E 29.1 m s^{-1}, NE 33.1 m s^{-1}, N 38.5 m s^{-1}, NW 42.6 m s^{-1}. Thus the strongest and deepest inflow occurs in the sector from northwest to southwest (i.e. the sector centred on the direction of storm motion) and the weakest and shallowest inflow in the sector southeast to east. These results are broadly consistent with the Kepert's findings. Note that, in contrast to Shapiro's study, there is inflow in all sectors, presumably because of the much stronger vortex here.

The strongest outflow lies in the south to southeast sector (panels (c) and (d) of Figure 11), which is broadly consistent also with Kepert's findings for Hurricane Georges.

Despite the good overall agreement with Kepert's observational study in the time-averaged fields, the fields at individual times show considerable variability between the 15 minute output times. For example panels (f) and (g) show the radial wind in the southeast to northwest sector at 162.5 h and 162.75 h, which should be compared with the corresponding time mean panel (d). At 162.5 h, the flow

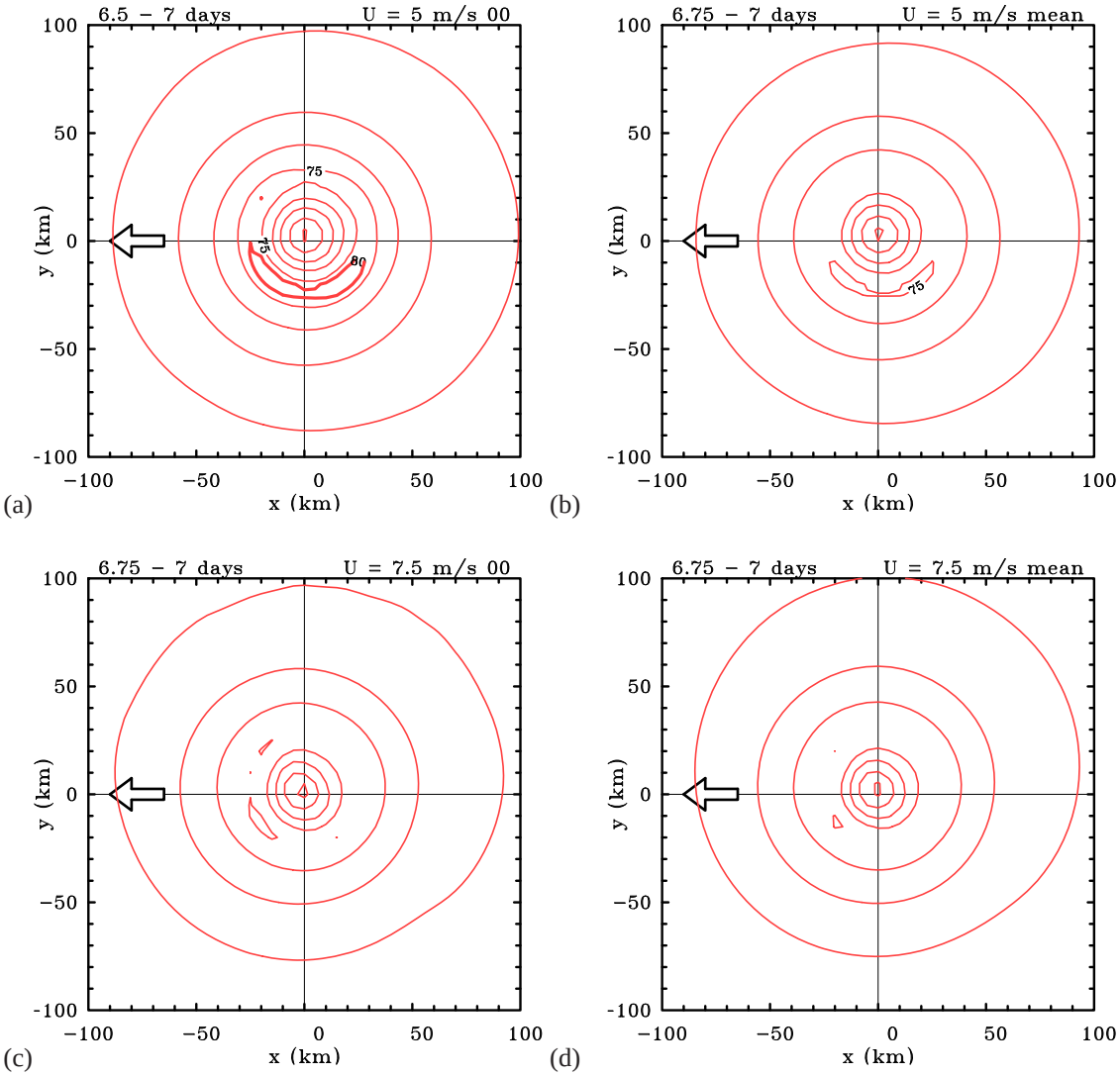

Figure 10. Contours of total wind speed at 850 mb averaged during the period $6\frac{3}{4} - 7$ days about the centre of minimum total wind speed at this level in a co-moving frame of reference in the control experiment and ensemble mean in the experiments with (a),(b) $U = 5$ m s^{-1}, and (c),(d) $U = 7.5$ m s^{-1}. Contour interval 15 m s^{-1} (thin contours). The thick contour in panel (a) has the value 80 m s^{-1}. The arrow indicates the direction of vortex motion.

from the northwest is strong and crosses the vortex centre, the maximum on this side being 54.0 m s^{-1}[‡]. In contrast, the maximum inflow on the southeastern side in this cross section is 28.3 m s^{-1}. Fifteen minutes later, the maximum inflow on the two sides of this cross section is comparable, but slightly larger on the southeastern side, 36.1 m s^{-1}, compared with 33.5 m s^{-1} on the northwestern side. One might argue that this extreme temporal variability is a reflection of the particular centre-finding method employed, but the variability in the centre position from a smooth track is simply a reflection of the presence of deep convection in the core that is responsible for the variability in the flow structures.

The foregoing structures are not captured in calculations that assume a *dry* symmetric translating vortex moving at uniform speed such as those of Shapiro *op. cit.* and Kepert (2006a,b). However, the extreme variability is supported by Kepert's analysis of observational data. For example, Kepert (2006a, p2178) states "The radial flow measurements show neither systematic variation nor consistency from profile to profile, possibly because the measurements were sampling small-scale, vertically-coherent, but transient features". Our calculations support this finding and suggest that the 'transient features' are associated with (vortical) deep convection.

At this time there does not appear to be a satisfactory theory to underpin the foregoing findings concerning the asymmetry in boundary layer depth. Of the two theories that we are aware of, Shapiro's (1983) study assumes a boundary layer of constant depth, but it does take into account an approximation to the nonlinear acceleration

[‡]While this inflow component may appear to be excessively large, we would argue that it is not unreasonable. For example, Kepert (2006a, Figure 9) shows mean profiles with inflow velocities on the order of 30 m s^{-1} for a vortex with a mean near-surface tangential wind speed of over 60 m s^{-1}. Moreover, Kepert (2006b, Figure 6) again on the order of 30 m s^{-1} with a mean near-surface tangential wind speed on the order of 50 m s^{-1}. Here the mean total near-surface wind speed is on the order of 75 m s^{-1}. The boundary layer composite derived from dropsondes released from research aircraft in Hurricane Isabel (2003) in the eyewall region by Montgomery *et al.* (2006) shows a similar ratio of 0.5 between the maximum mean near-surface inflow to maximum near-surface swirling velocity. The recent dropsonde composite analysis of many Atlantic hurricanes by Zhang *et al.* (2011b) confirms that a ratio of 0.5 for the mean inflow to mean swirl for major hurricanes appears to be typical near the surface.

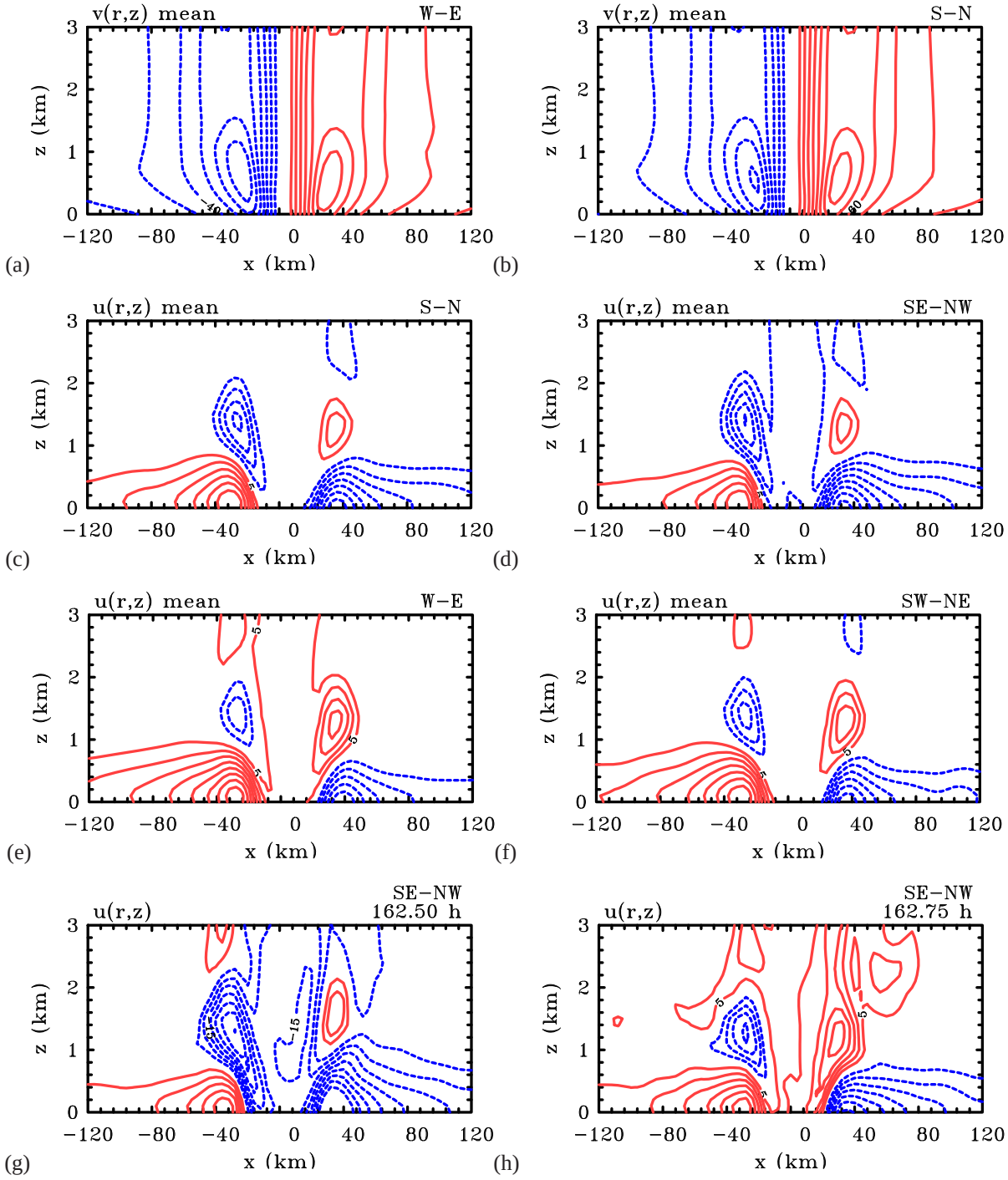

Figure 11. Height-radius cross sections showing the isotachs of the wind components in and normal to different compass directions (x) in the co-moving frame. The data are for the control calculation with $U = 5$ m s^{-1} and are averaged over the last 6 hours of the calculation. Normal component to the cross section: (a) west to east, (b) south to north. Component in the cross section: (c) south to north, (d) southeast to northwest, (e) west to east, (f) southwest to northeast. Panels (g) and (h) show the radial wind at two particular times, 15 minutes apart, during the last six hours. Contour values: 10 m s^{-1} for normal (tangential) wind, 5 m s^{-1} for the wind component in the cross section. Positive contours are denoted by solid/red and negative contours are denoted by dashed/blue.

terms in the inner core of the vortex. In contrast, Kepert (2001) presents a fully linear theory that accounts for the variation of the wind with height through the boundary layer and the variation of boundary-layer depth with azimuth, but the formulation invokes approximations whose validity are not entirely clear to us. For example, he assumes that the background steering flow is in geostrophic balance, but notes that "the asymmetric parts of the solution do not reduce to the Ekman limit for straight flow far from the vortex". In addition, he assumes that the tangential wind speed is large compared with the background flow speed, an assumption that restricts the validity of the asymmetric component to the inner-core region of the vortex. However, this is precisely the region where linear theory for both the symmetric flow component (Vogl and Smith 2009) and asymmetric flow component (Shapiro, 1983 - see his Table II) cannot be formally justified. Thus it is difficult for us to precisely identify a region in which the theory might be applicable.

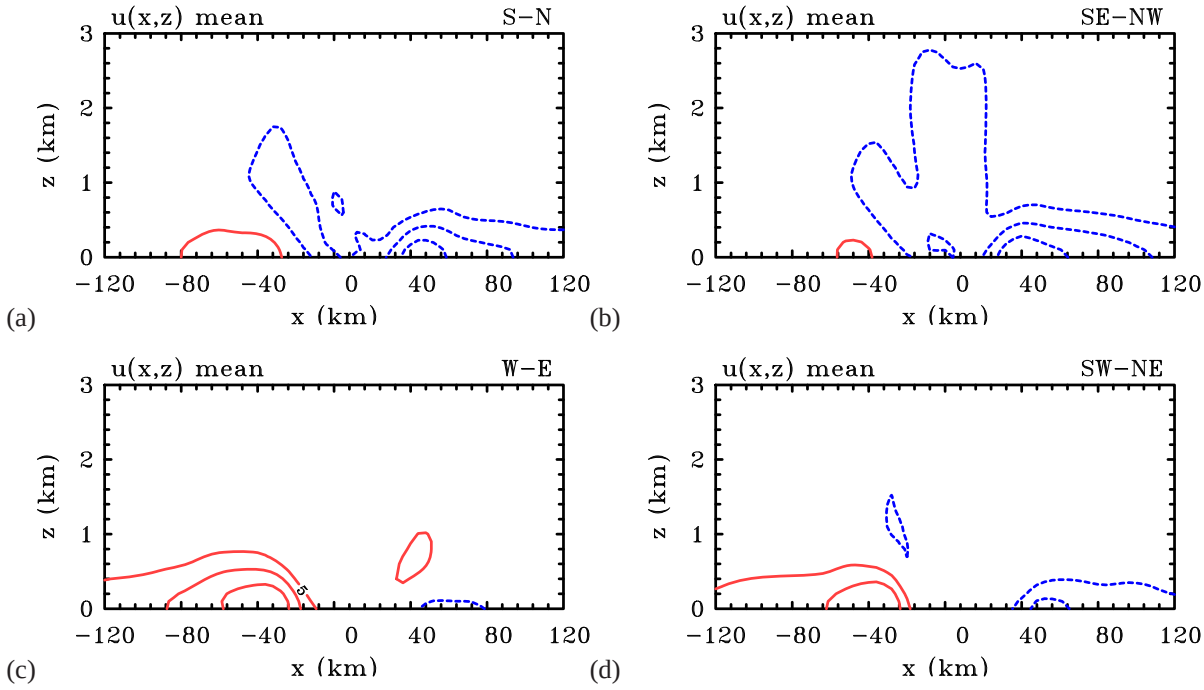

Figure 12. Height-radius cross sections showing isotachs of the wind component in different compass directions (x) in the co-moving frame. The data are for the control calculation with $U = 5$ m s^{-1} and a sea surface temperature of 25^{o}C, and are averaged over the last 6 hours of the calculation. (a) south to north, (b) southeast to northwest, (c) west to east, (d) southwest to northeast. Contour values: 5 m s^{-1}. Positive contours solid/red, negative contours dashed/blue.

In general terms, one might argue that where the boundary-layer wind speeds are largest, the boundary-layer depth would be shallowest since the local Reynolds number is largest in such regions. However, such an argument assumes that the eddy diffusivity does not change appreciably with radius. The results of Braun and Tao (2001, see their Figure 15) imply that this assumption cannot be justified in general, and those of Smith and Thomsen (2010) show that it is not justified even when there is no background flow (see their Figure 8).

As shown in Figure 12, the variation in the radius-height patterns of the time-mean inflow do not change appreciably in the case of a weaker vortex, but the magnitude of the radial flow is weaker than for the stronger vortex (compare panels (a) to (d) of Figure 12 with panels (c) - (f) of Figure 10, respectively).

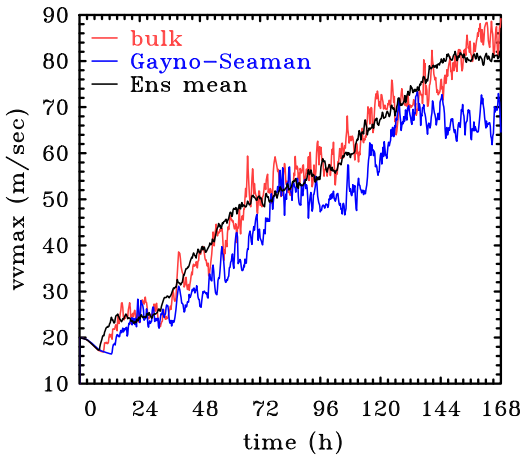

Figure 13. Time series of maximum total wind speed at 850 mb for the control experiments with $U = 5.0$ m s^{-1} (bulk/red curve), the corresponding ensemble mean (Ens mean/black curve) and the experiment using the Gayno-Seaman boundary-layer scheme (blue curve).

6. The Gayno-Seaman boundary-layer scheme

The foregoing calculations are based on one of the simplest representations of the boundary layer. It is therefore pertinent to ask how the results might change if a more sophisticated scheme were used. A comparison of different schemes in the case of a quiescent environment was carried out by Smith and Thomsen (2010), where it was found that the bulk scheme used here is one of the least diffusive. For this reason we repeated the main calculation with $U = 5$ m s^{-1} with the bulk scheme replaced by the Gayno-Seaman scheme. The latter is one of the more diffusive schemes examined by Smith and Thomsen (2010), giving a maximum eddy diffusivity, K, of about 250 m^2 s^{-1}. This value is considerably larger than the maximum found so far in observations[§] suggesting that this scheme may be unrealistically diffusive.

Figure 13 compares the evolution of the maximum total wind speed at 850 mb for this case with that in the main calculation for $U = 5$ m s^{-1} and with that for the corresponding ensemble mean. As expected from the results of Smith and Thomsen *op. cit.*, the use of this scheme

[§]The only observational estimates for this quantity that we are aware of are those analysed recently from flight-level wind measurements at an altitude of about 500 m in Hurricanes Allen (1980) and Hugo (1989) by Zhang *et al.* (2011a). In Hugo, maximum K-values were about 110 m^2 s^{-1} beneath the eyewall, where the near-surface wind speeds were about 60 m s^{-1}, and in Allen they were up to 74 m^2 s^{-1}, where wind speeds were about 72 m s^{-1}.

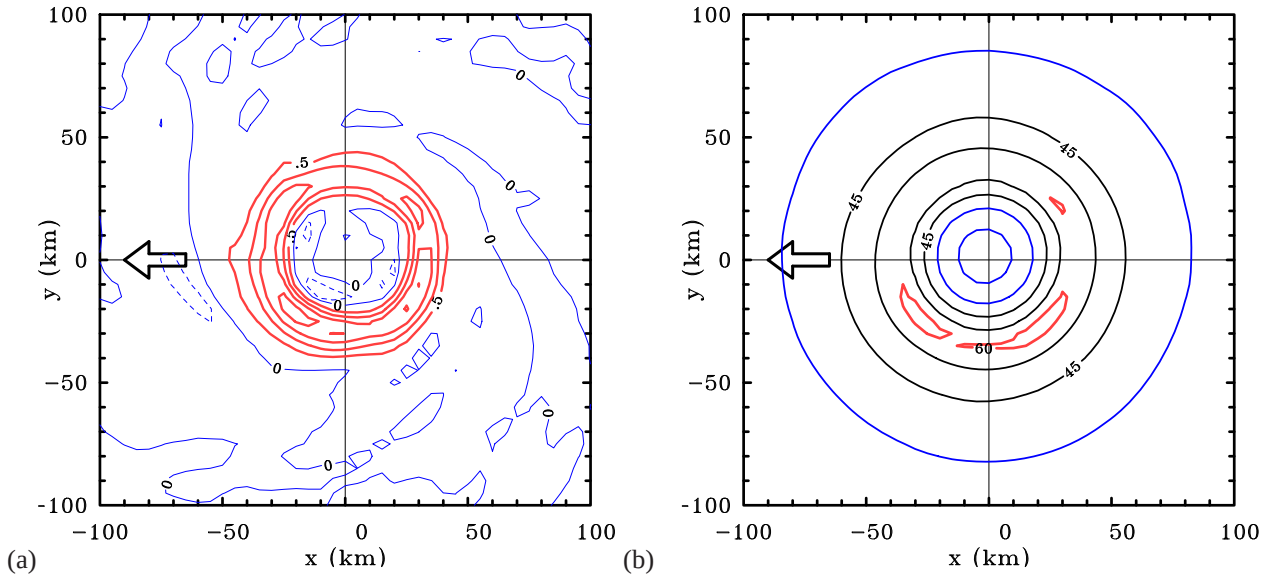

Figure 14. Contours of (a) vertical velocity, and (b) total wind speed at 850 mb averaged during the period $6\frac{3}{4} - 7$ days about the centre of minimum total wind speed at this level in the experiment with $U = 5.0$ m s^{-1} which uses the Gayno-Seaman boundary-layer parameterization scheme. The arrow indicates the direction of vortex motion.

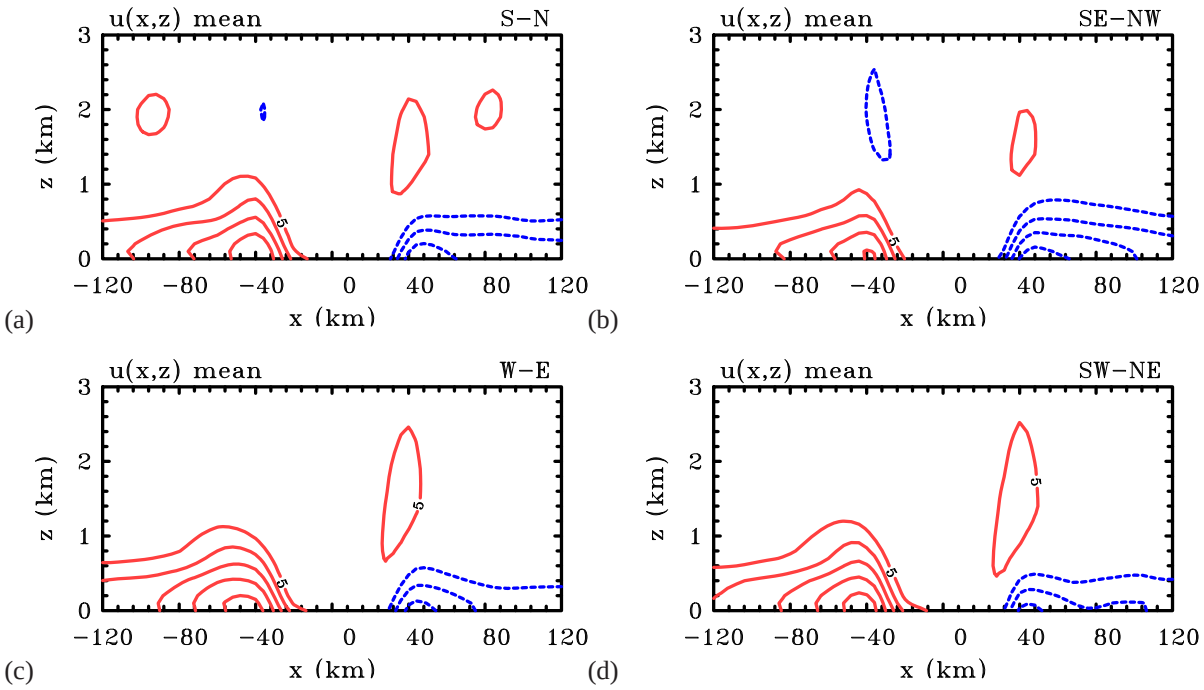

Figure 15. Height-radius cross sections showing isotachs of the wind component in different compass directions (x) in the co-moving frame. The data are for the control calculation with $U = 5$ m s^{-1} and with the Gayno-Seaman boundary-layer scheme, and are averaged over the last 6 hours of the calculation. (a) south to north, (b) southeast to northwest, (c) west to east, (d) southwest to northeast. Contour values: 5 m s^{-1}. Positive contours solid/red, negative contours dashed/blue.

leads to a reduced intensification rate and a weaker vortex in the mature stage. However, as shown in Figure 14, the patterns of the wind and vertical velocity asymmetries are similar to those with the bulk scheme (compare Figure 14a with Figure 8d and Figure 14b with Figure 10a). Of course, the maxima of the respective fields are weaker. The same remarks apply also to the vertical cross-sections of radial inflow shown in Figure 15. As in the corresponding calculation with the bulk scheme, the deepest and strongest inflow occurs on the downstream (western) side of the vortex and the weakest is on the upstream side (compare the panels in Figure 15 with the corresponding panels (c), (d), (e) and (f) in Figure 11). More generally, the inflow is strongest in the sector from northwest to south and weakest in that from southeast to north, but the magnitudes are smaller than with the bulk scheme.

7. Conclusions

We have presented an analysis of the dynamics of tropical-cyclone intensification in the prototype problem for a moving tropical cyclone using a three-dimensional numerical model. The problem considers the evolution of

an initially dry, axisymmetric vortex in hydrostatic and gradient wind balance, embedded in a uniform zonal flow on an f-plane. The calculations naturally extend those of Nguyen *et al.* (2008), who examined tropical-cyclone intensification in a quiescent environment.

The calculations were motivated in part by our desire to answer four basic questions. The first is: does the imposition of a uniform flow lead to an organization of the inner-core convection making its distribution more predictable relative to the case of a quiescent environment? The answer to this question is a qualified yes. For the relatively strong vortices mostly studied here, the effect is pronounced only for the maximum background flow studied (7.5 m s^{-1}). In this case we found that the time-averaged vertical velocity field at 850 mb during the last six hours of the calculations has a maximum at about 45^o to the left of the vortex motion vector. This maximum survives also in the ensemble mean, suggesting that it is a robust feature and not just a transient one associated with a particular convective cell.

In an Earth-relative frame, the total wind has a maximum in the forward right quadrant, a feature that survives also in the ensemble mean calculation. In the co-moving frame, this maximum moves to the forward left quadrant in the ensemble mean.

The low-level asymmetric wind structure found above remains unaltered when the more sophisticated, but more diffusive Gayno-Seaman scheme is used to represent the boundary layer. We conclude that our results are not overly sensitive to the boundary-layer scheme used.

The three other questions addressed concern the relation of our results to previous studies. First, does the imposition of a uniform flow significantly affect the intensification rate and mature intensity for storm translation speeds typical of those in the tropics? Again, for the relatively strong vortices mostly studied here, our results suggest that the answer is no, because there is considerably overlap between ensemble members in the sets of calculations for different wind speeds. When viewed in the proper way, we showed that these results are consistent with the analyses of observational data presented by Zeng *et al.* (2007).

Second, to what extent do our results corroborate with those of previous theoretical investigations? A useful metric for comparing the results is via the vortex-scale pattern of horizontal convergence/divergence at the top of the boundary layer. We find that the direction of the maximum is about 45^o to the left of that predicted by Shapiro (1983), where the maximum convergence is in the direction of motion. This difference may have consequences for the interpretations of observations, since Shapiro's results are frequently invoked as a theoretical benchmark for characterizing the boundary-layer induced vertical motion (e.g. Corbosiro and Molinari (2003, p375). The direction of the maximum convergence is significantly different from that in Kepert's (2001) linear theory, where the maximum vertical motion is 45^o to the right of vortex motion, and even more different from that in the nonlinear numerical calculation of Kepert and Wang (2001), where the maximum is at 90^o to the right of the motion vector. The reasons for these discrepancies are unclear to us, but they could be, at least in part, because in our calculations, the vortex flow above the boundary layer is determined as part of a full solution for the flow and not prescribed.

The final question raised is: how well do the findings compare with recent observations of boundary-layer flow asymmetries in translating storms by Kepert (2006a,b) and Schwendike and Kepert (2008)? We found that vertical cross sections of the 6 hour averaged, storm-relative, tangential wind component in the lowest 3 kilometres during the mature stage show a slight tendency for the maximum tangential wind component to become lower in altitude with decreasing radius as the radius of the maximum tangential wind is approached. Moreover, the maximum tangential wind speed occurs on the left (i.e. southern) side of the storm as is found in the observations reported by in the foregoing papers. Similar cross sections of the radial wind component show that the strongest and deepest inflow occurs in the sector from northwest to southwest (i.e. in the direction of storm motion) and the weakest and shallowest inflow in the sector southeast to east, consistent also with the observations. In contrast, the radial wind component at individual times during the mature stage shows considerable variability on a 15 minute time scale, apparently because of the variability of deep convection on this time scale. This result raises a potential issue concerning the ability to determine asymmetries in the radial inflow from dropwindsonde observations spread over several hours.

8. Acknowledgements

GLT and RKS were supported in part by the German Research Council (DFG). MTM acknowledges the support of Grant No. N0001411Wx20095 from the U.S. Office of Naval Research and NSF AGS-0733380 and NSF AGS-0851077, NOAAs Hurricane Research Division and NASA grants NNH09AK561 and NNG09HG031.

References

Black PG D'Asoro EA Drennan WM French JR Niller PP Sanford TB Terril EJ Walsh EJ Zhang JA 2007 Air-sea exchange in hurricanes. Synthesis of observations from the coupled boundary layer air-sea transfer experiment. *Bull. Amer. Meteorol. Soc.*, **88,** 357-374.

Corbosiero KL Molinari J. 2002 The effects of vertical wind shear on the distribution of convection in tropical cyclones. *Mon. Wea. Rev.*, **130**, 2110-2123.

Corbosiero KL Molinari J. 2003 The relationship between storm motion, vertical wind shear, and convective asymmetries in tropical cyclones. *J. Atmos. Sci.*, **60**, 366-376.

Dengler K Keyser D. 2000 Intensification of tropical cyclone-like vortices in uniform zonal background flows. *Q. J. R. Meteorol. Soc.*, **126**, 549-568.

Dudhia J. 1993 A non-hydrostatic version of the Penn State-NCAR mesoscale model: Validation tests and simulation of an Atlantic cyclone and cold front. *Mon. Wea. Rev.*, **121**, 1493-1513.

Frank WM Ritchie EA. 1999 Effects of environmental flow on tropical cyclone structure. *Mon. Wea. Rev.*, **127**, 2044-2061.

Frank WM Ritchie EA. 2001 Effects of vertical wind shear on the intensity and structure of numerically simulated hurricanes. *Mon. Wea. Rev.*, **129**, 2249-2269.

Grell GA Dudhia J and Stauffer DR. 1995 A description of the fifth generation Penn State/NCAR mesoscale model (MM5). NCAR Tech Note NCAR/TN-398+STR, 138 pp.

Hendricks EA Montgomery MT Davis CA. 2004 On the role of "vortical" hot towers in formation of tropical cyclone Diana (1984). *J. Atmos. Sci.*, **61**, 1209-1232.

Jones SC. 1995 The evolution of vortices in vertical shear. Part I: Initially barotropic vortices. *Q. J. R. Meteorol. Soc.*, **121**, 821851.

Jones SC. 2000a: The evolution of vortices in vertical shear. II: Large-scale asymmetries. *Q. J. R. Meteorol. Soc.*, **126**, 3137-3160.

Jones SC. 2000b: The evolution of vortices in vertical shear. III: Baroclinic vortices. *Q. J. R. Meteorol. Soc.*, **126**, 3161-3186.

Jordan CL. 1958 Mean soundings for the West Indies area. *J. Meteor.*, **15,** 91-97.

Kepert JD. 2001 The dynamics of boundary layer jets within the tropical cyclone core. Part I: Linear Theory. *J. Atmos. Sci.*, **58,** 2469-2484.

Kepert JD Wang Y. 2001 The dynamics of boundary layer jets within the tropical cyclone core. Part II: Nonlinear enhancement. *J. Atmos. Sci.*, **58,** 2485-2501.

Kepert JD. 2006a Observed boundary-layer wind structure and balance in the hurricane core. Part I. Hurricane Georges. *J. Atmos. Sci.*, **63,** 2169-2193.

Kepert JD. 2006b Observed boundary-layer wind structure and balance in the hurricane core. Part II. Hurricane Mitch. *J. Atmos. Sci.*, **63,** 2194-2211.

Montgomery MT Bell MM Aberson SD and Black ML. 2006b Hurricane Isabel (2003): New insights into the physics of intense storms. Part I Mean vortex structure and maximum intensity estimates. *Bull. Amer. Meteorol. Soc.*, **87**, 1335 - 1348.

Nguyen SV Smith RK and Montgomery MT. (M1) 2008 Tropical-cyclone intensification and predictability in three dimensions. *Q. J. R. Meteorol. Soc.*, **134**, 563-582.

Peng MS Jeng B-F Williams RT. 1999 A numerical study on tropical cyclone intensification. Part I: Beta effect and mean flow effect. *J. Atmos. Sci.*, **56**, 1404-1423.

Raymond DJ. 1992 Nonlinear balance and potential-vorticity thinking at large Rossby number. *Q. J. R. Meteorol. Soc.*, **118**, 987-1015.

Reasor PD Montgomery MT. 2001 Three-dimensional alignment and co-rotation of weak TC-like vortices via linear vortex Rossby waves. *J. Atmos. Sci.*, **58**, 2306-2330.

Schwendike J Kepert JD. 2008 The boundary layer winds in Hurricane Danielle (1998) and Isabel (2003). *Mon. Wea. Rev.*, **136**, 3168-3192.

Shafran PC Seaman NL and Gayno GA. 2000 Evaluation of numerical predictions of boundary layer structure during the lake Michigan ozone study. *J. Appl. Met.*, **39**, 337-351.

Shapiro LJ. 1983 The asymmetric boundary layer flow under a translating hurricane. *J. Atmos. Sci.*, **40**, 1984-1998.

Shin S Smith RK. 2008 Tropical-cyclone intensification and predictability in a minimal three-dimensional model. *Q. J. R. Meteorol. Soc.*, **134**, 1661-1671.

Smith RK. 2006 Accurate determination of a balanced axisymmetric vortex. *Tellus*, **58A**, 98-103.

Smith RK Ulrich W Sneddon G. 2000 On the dynamics of hurricane-like vortices in vertical shear flows. *Q. J. R. Meteorol. Soc.*, **126**, 2653-2670.

Smith RK and Thomsen GL. 2010 Dependence of tropical-cyclone intensification on the boundary layer representation in a numerical model. *Q. J. R. Meteorol. Soc.*, **136**, 1671-1685.

Weckwerth TM. 2000 The effect of small-scale moisture variability on thunderstorm initiation. *Mon. Wea. Rev.*, **128**, 4017-4030.

Wu L Braun SA. 2004 Effects of environmentally induced asymmetries on hurricane intensity: A numerical study. *J. Atmos. Sci.*, **61**, 3065-3081.

Zhang D-L Liu Y Yau MK. 2001 A multi-scale numerical study of Hurricane Andrew (1992). Part IV: Unbalanced flows. *Mon. Wea. Rev.*, **129**, 92-107.

Zhang J Drennan WM Black PB French JR. 2009 Turbulence structure of the hurricane boundary layer between the outer rainbands. *J. Atmos. Sci.*, **66**, 2455-2467.

Zhang JA Marks FD Montgomery MT and Lorsolo S. 2011a An estimation of turbulent characteristics in the low-level region of intense Hurricanes Allen (1980) and Hugo (1989). *Mon. Wea. Rev.*, **139**, 1447-1462.

Zhang JA Rogers RF Nolan DS and Marks FD. 2011b On the characteristic height scales of the hurricane boundary layer. *Mon. Wea. Rev.*, **139**, 2523-2535.

Zeng Z Wang Y Wu C-C. 2007 Environmental dynamical control of tropical cyclone intensity - An observational study. *Mon. Wea. Rev.*, **135**, 38-59.